Electronic structure of nanoporous ceria from x-ray absorption spectroscopy and atomic multiplet calculations

S. O. Kucheyev,* B. J. Clapsaddle,† Y. M. Wang, T. van Buuren, and A. V. Hamza
Nanoscale Synthesis and Characterization Laboratory, Lawrence Livermore National Laboratory, Livermore, California 94551, USA
(Received 22 February 2007; revised manuscript received 21 August 2007; published 19 December 2007)

We study the electronic structure of three-dimensional nanoporous CeO_{2-x} monoliths (aerogels) by soft x-ray absorption near-edge structure (XANES) spectroscopy. Atomic multiplet calculations are used to interpret high-resolution Ce $M_{4,5}$- and $N_{4,5}$-edge XANES spectra. Results show that aerogels with thicker ligaments, but with the same average size of crystallites, exhibit larger Ce^{3+} content and, hence, higher oxygen deficiency.

DOI: 10.1103/PhysRevB.76.235420 PACS number(s): 71.20.Eh, 78.70.Dm, 71.55.Ht, 82.70.Gg

I. INTRODUCTION

Cerium compounds are the best studied rare earths due to their technological importance and the interesting physical properties inherent to the *f*-electron systems.[1] For example, metallic cerium has attracted significant research interest primarily because it exhibits some properties similar to those of Pu. Cerium oxides find many technological applications, including catalysts, solid oxide fuel cells, and ultraviolet absorbers. Most of these applications strongly depend on the electronic properties, which involve largely localized or delocalized 4*f* electron states, as in Ce_2O_3 and CeO_2, respectively.[2]

Recently, there have been numerous reports on nanostructured cerium oxides, with a major focus on an increase in the surface area to boost their catalytic efficiency (see, for example, Refs. 3–9). One approach to the synthesis of nanostructured ceria is the sol-gel process. Several recipes for sol-gel-derived ceria nanomaterials and aerogels (AGs), in particular, have been reported.[6–9] Such AGs are open-cell nanoporous solids derived from highly cross-linked wet gels by drying them under supercritical conditions.[10] However, the technologically important electronic structure of sol-gel-derived nanoporous ceria remains essentially unexplored.

In this paper, we study the electronic structure of ceria AGs recently synthesized in our laboratory.[11] We use soft x-ray absorption near-edge structure (XANES) spectroscopy around Ce $M_{4,5}$ (excitation of Ce 3*d* core levels) and $N_{4,5}$ (excitation of Ce 4*d* core levels) edges in combination with atomic multiplet calculations based on a simplified Anderson impurity model.[12] Our results show that the Ce^{3+}/Ce^{4+} ratio in AGs could be correlated with the average width of the nanoligaments in the three-dimensional solid network of AGs.

II. EXPERIMENTS AND MULTIPLET CALCULATIONS

Ceria AGs were prepared based on a general epoxide-initiated gelation method developed in our laboratory.[13] The details of the synthesis of the entire lanthanide series of AGs will be described elsewhere.[11] Ceria gel synthesis was performed by dissolving 1.1 g (3.0 mmol) of $CeCl_3 \cdot 7H_2O$ in 5 g of methanol. Following dissolution, 1.6 g (28 mmol) of propylene oxide was added to the solution, which was allowed to gel. Gelation was defined as the point at which the viscous reaction sol ceased to discernibly flow under the influence of gravity. The two gels prepared in this study, labeled "AG3" and "AG4," had gelation times of ~150 and ~110 minutes, respectively. Following gelation, the wet gels were allowed to age for 24 h under ambient conditions. Gels were then solvent exchanged by immersion in a bath of absolute ethanol, where they were exchanged 3 times in 3 days, changing the ethanol daily. The wet gels were dried to AGs in a Polaron™ supercritical point drier. The alcohol in the gel pores was exchanged for liquid CO_2 for 2–3 days at ~12 °C, after which the temperature of the vessel was ramped up to ~45 °C while maintaining a pressure of ~100 bar. The vessel was then depressurized at a rate of ~7 bar/hour.

The resultant AGs had a Brunauer-Emmett-Teller surface area of ~250 $m^2\,g^{-1}$, an average Barrett-Joyner-Halenda pore diameter of 25 nm, and a pore volume of 1.5 ml g^{-1}. The microstructure was studied by transmission electron microscopy (TEM) (at 300 kV). As reference Ce^{3+} and Ce^{4+} compounds, we used $CeCl_3$ and CeO_2 powders (with grain sizes $\gtrsim 5$ μm and purities of 99.50% and 99.99%, respectively), obtained from Alfa Aesar.

The XANES experiments were performed at undulator beamline 8.0 at the Advanced Light Source. Spectra were obtained by measuring the total electron yield (TEY) by monitoring the total sample photocurrent normalized to the incoming radiation flux. The overall experimental resolution around Ce 3*d* ($M_{4,5}$) and 4*d* ($N_{4,5}$) edges was ~0.2 and ~0.1 eV, respectively. After a linear background subtraction, all spectra were normalized to the intensity integrated over the entire edge and multiplied by the number of *f*-shell vacancies in the ground state (i.e., by factors of 13 and 14 for Ce^{3+} and Ce^{4+}, respectively). This was performed since a more common postedge step height normalization procedure[14] resulted in nonreproducible total intensities, which we attribute to sample charging effects.

Atomic multiplet calculations of Ce 3*d* and 4*d* core-level spectra were done with a version of Cowan's code[15] modified by Thole *et al.*[16] This code takes into account Coulomb, exchange, and spin-orbit interactions.[12] Crystal field effects were not included in calculations since they are typically negligible for the 4*f* systems.[1] In order to fit experimental Ce $M_{4,5}$ spectra for both Ce^{3+} and Ce^{4+}, the $4f-4f$ Slater-

Condon parameters were reduced to 70% and the $3d$ spin-orbit parameters to 96% of their Hartree-Fock values. To fit experimental $N_{4,5}$ spectra of both Ce^{3+} and Ce^{4+}, the $4f-4f$ and $4d-4f$ exchange Slater-Condon parameters (G_i) were reduced to 60% and 80%, respectively, while $4d$ and $4f$ spin-orbit parameters were reduced to 95% and 90%, respectively. Such a reduction of Slater-Condon parameters effectively takes into account bond covalency.

It was necessary to include charge transfer effects with mixed $4f^0+4f^1$ ground and $4f^1+4f^2$ final states in order to match experimental spectra for Ce^{4+}, while the spectra for Ce^{3+} were described well with calculations assuming the $4f^1$ ground state. The best fit between theory and experiment was obtained with the following parameters for the Ce^{4+} mixed-valence state:[12] an energy difference between the $4f^0$ and $4f^1$ configurations of the ground state of 2 eV and between the $4f^1$ and $4f^2$ configurations of the exited state of 1 eV, and the mixing parameters for the ground and excited states of 0.3 and 0.85, respectively. The ligand hole bandwidth was 2 eV.

For a better comparison with experimental data, lifetime broadening was taken into account by convoluting multiplet lines with Lorentzians with full widths at half maximum of 0.2 eV and 0.4 eV for M_5 and M_4 edges, respectively, and of 0.05 eV and 3.0 eV for sharp and broad (sometimes called "giant") regions of the $N_{4,5}$ multiplet structure, respectively, for both Ce^{3+} and Ce^{4+} spectra. Gaussian broadening (with standard deviations of 0.2 and 0.1 eV for $M_{4,5}$ and $N_{4,5}$ spectra, respectively) was applied to account for instrumental broadening effects.

The major difference between our multiplet calculations and those reported previously[16–20] is that we model both Ce^{3+} and Ce^{4+} for both $M_{4,5}$ and $N_{4,5}$ edges with the same main set of parameters, optimizing them to fit high-resolution experimental spectra. As a result, the details of the spectral features in the theoretical spectra presented here are different from those reported previously.[16–20]

III. RESULTS AND DISCUSSION

Below, we discuss the properties of two representative AGs (labeled AG3 and AG4) prepared under identical major conditions, including the precursor, solvent, gelation agent, and their concentrations. The only difference in the preparation conditions of these AGs was the gelation time, as discussed in the previous section. Our results clearly illustrate a large flexibility of the sol-gel synthesis, where subtle differences in preparation conditions can dramatically change the structure of the resultant nanomaterial.

The morphology of these two representative AGs is illustrated in low-magnification TEM images in Figs. 1(a) and 1(b), showing that the AG skeleton is formed by interconnected ligaments with average widths of ~5 and ~10 nm for AGs labeled AG4 and AG3, respectively. Also shown in Fig. 1 by dotted lines are representative ligaments [Figs. 1(a) and 1(b)] and crystallites [Figs. 1(c) and 1(d)]. Figure 2 shows distributions of widths of crystallites [Fig. 2(a)] and ligaments [Fig. 2(b)] in AG3 and AG4, obtained from a statistical analysis of TEM images such as shown in Fig. 1. It is seen from Figs. 1 and 2 that the AG3 monolith, which took longer to gel, has wider ligaments than the AG4 gel. Selected-area electron diffraction analysis indicates that the nanoligaments in both AGs are crystalline with a cubic fluorite lattice ($Fm3m$) in which full-density CeO_2 crystallizes [see insets in Figs. 1(c) and 1(d)]. It is important to mention that both AGs with different average ligament widths (of ~5 and ~10 nm) have almost the same average diameters of crystallites of ~5 nm (Figs. 1 and 2).

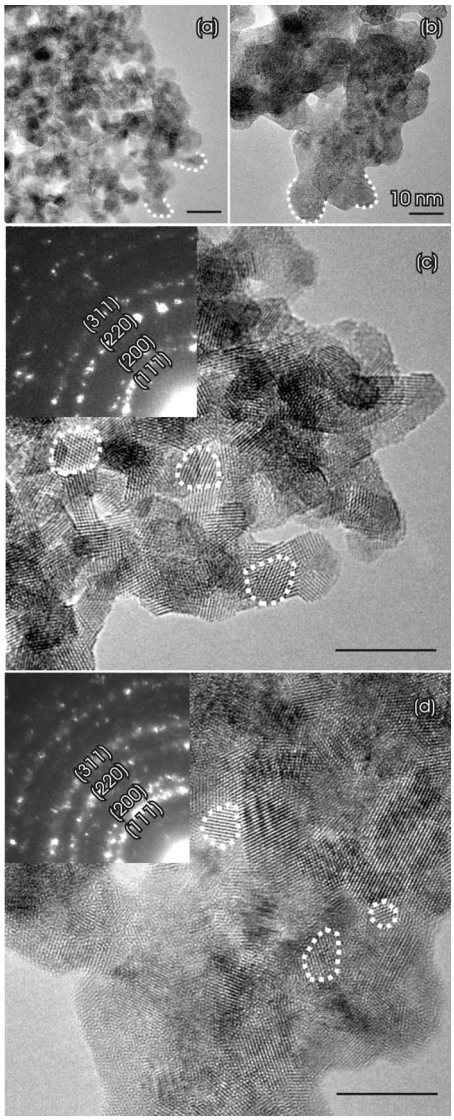

FIG. 1. Bright-field TEM images, taken under two different magnifications, of two representative CeO_{2-x} aerogels, labeled [(a) and (c)] AG4 and [(b) and (d)] AG3, illustrating that they are formed by a continuous network of ceria nanoligaments of different widths but with crystallites with similar average diameters of ~5 nm. Scale bars are 10 nm in all four images. Representative ligaments and crystallites are shown by dotted lines in (a) and (b) and (c) and (d), respectively. Selected-area diffraction patterns from AG4 and AG3 are shown in insets in (c) and (d), respectively.

Figure 3(b) shows Ce $M_{4,5}$-edge XANES spectra of AGs and full-density CeO_2 and $CeCl_3$. Such spectra reflect electron transitions from the Ce $3d$ core levels into $4f$ unoccupied electronic states above the Fermi level. However, these

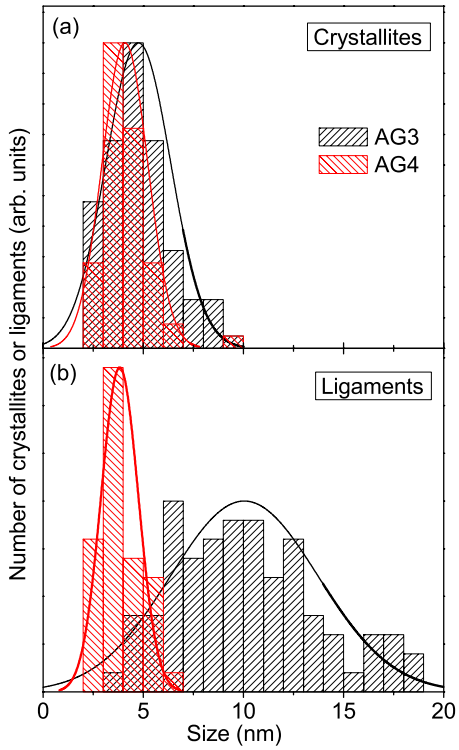

FIG. 2. (Color online) Distributions of widths of (a) crystallites and (b) ligaments in two representative ceria aerogels labeled AG3 and AG4.

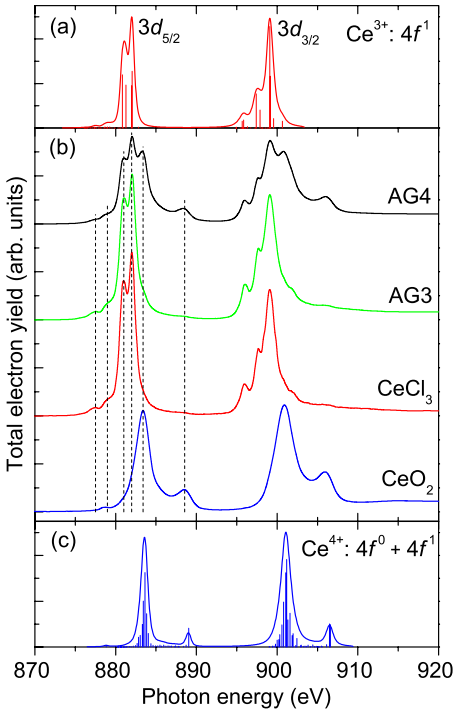

FIG. 3. (Color online) Cerium $M_{4,5}$-edge XANES spectra for two representative ceria aerogels (labeled AG3 and AG4) and reference compounds. Experimental data are shown in (b) and results of atomic multiplet calculations for Ce^{3+} and Ce^{4+} in (a) and (c), respectively.

spectra reflect multiplet effects rather than the density of states in the conduction band. Such multiplet effects are caused primarily by a strong interaction of the $3d$ core hole and $4f$ states. Hence, in order to interpret these spectra, we have performed atomic multiplet calculations, as described in the previous section. Figures 3(a) and 3(c) show the results of such multiplet calculations for Ce^{3+} and Ce^{4+}, respectively. Excellent agreement is seen between theoretical and experimental spectra for CeO_2 and $CeCl_3$, where Ce atoms have formal oxidation states of 4+ and 3+, respectively. A comparison of $M_{4,5}$-edge spectra accumulated consecutively from the same area of the sample reveals no evidence of any effects of x-ray-induced damage, often believed to influence XANES spectra of Ce compounds.[21]

Figure 3 also shows that the spectrum for AG3, which has thicker ligaments than AG4, is almost indistinguishable from that for Ce^{3+}, indicating that Ce is predominantly in the 3+ oxidation state in AG3. The spectrum for AG4 reveals a mixture of Ce^{3+} and Ce^{4+}, with no other peaks in addition to the multiplet features characteristic of these two oxidation states. A quantitative analysis by fitting $M_{4,5}$ spectra from AGs with weighted spectra from CeO_2 and $CeCl_3$ suggests Ce^{3+} contents of ~95% and ~40% in AG3 and AG4, respectively.

The finding that AGs with thicker ligaments have higher Ce^{3+} content is further supported by Ce $N_{4,5}$-edge XANES spectra illustrated in Fig. 4(b). Results of multiplet calculations for $N_{4,5}$ edges of Ce^{3+} and Ce^{4+} are shown in Figs. 4(a) and 4(c), respectively. Due to large direct and exchange interactions of strongly overlapping $4d$ and $4f$ wave functions and relatively small spin-orbit coupling of $4d$ and $4f$ electrons, such $N_{4,5}$-edge spectra cannot be separated into N_4 and N_5 edges; i.e., into contributions from $4d_{3/2} \rightarrow 4f$ and $4d_{5/2} \rightarrow 4f$ transitions. The $N_{4,5}$-edge multiplet peaks are, however, clearly separated into two groups: (i) sharp, low-intensity "dipole-forbidden" (and allowed due to spin-orbit-induced mixing with dipole-allowed final states at higher energies) transitions at $\lesssim$115 eV and (ii) broad, high-intensity "dipole-allowed" (hence, carrying most of the oscillator strength) transitions at higher energies. Note that both sharp and broad peaks are parts of the same multiplet structure. The difference in the width of these two groups of peaks is due to short lifetimes of the higher-energy final states, which is related to a very efficient $4d^9 4f^2 \rightarrow 4d^{10} 4f^0 + e$ autoionization process (which is also consistent with the f^1 and $f^0 + f^1$ ground states of Ce^{3+} and Ce^{4+}, respectively, assumed in our multiplet calculations).[21–23]

Data from Fig. 4 are in agreement with our $M_{4,5}$-edge analysis (Fig. 3), showing that AG3 exhibits predominantly Ce^{3+} features, while the spectrum of AG4 has both Ce^{3+} and Ce^{4+} peaks. Fitting such $N_{4,5}$ spectra from AGs with weighted spectra from CeO_2 and $CeCl_3$ suggests Ce^{3+} contents of ~90% and ~50% in AG3 and AG4, respectively. These values are in reasonable agreement with those obtained from fitting $M_{4,5}$ spectra.

It is interesting to note that the number and energy positions of sharp multiplet peaks at $\lesssim$115 eV in Fig. 4(b) are the same for all the samples studied, including even the CeO_2 reference powder, and are characteristic of Ce^{3+} rather than Ce^{4+}.[24–26] However, the structure of intense broad peaks

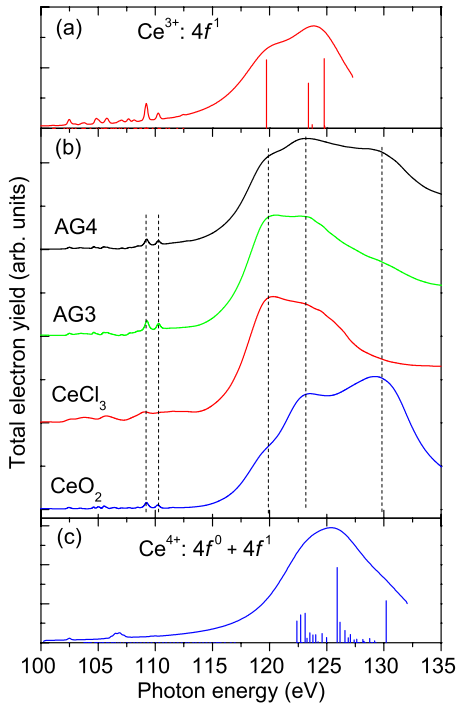

FIG. 4. (Color online) Cerium $N_{4,5}$-edge XANES spectra for two representative ceria aerogels (labeled AG3 and AG4) and reference compounds. Experimental data are shown in (b) and results of atomic multiplet calculations for Ce^{3+} and Ce^{4+} in (a) and (c), respectively. The vertical lines in (a) and (c) were normalized by factors of 7 and 5, respectively.

at $\gtrsim$115 eV varies significantly for different Ce compounds, with broad peaks centered on ~120 and ~129 eV being representative of Ce^{3+} and Ce^{4+}, respectively. The fact that the lower energy part of the multiplet structure is Ce^{3+}-like for all the samples could be attributed to effects of x-ray-induced damage.[21,26] The fact that x-ray damage effects are observed in $N_{4,5}$-edge (Fig. 4) and not in $M_{4,5}$-edge (Fig. 3) spectra could be attributed to (i) about an order of magnitude larger photon flux,[27,28] (ii) $\lesssim$3 times larger x-ray absorption cross section,[29] and (iii) about an order of magnitude smaller TEY probing depth[30,31] at ~100 eV (Ce $N_{4,5}$ edge) than at ~900 eV (Ce $M_{4,5}$ edge).

Data from Fig. 4 could also suggest that the $4d \rightarrow 4f$ transitions in the dipole-forbidden regime are significantly more intense for Ce^{3+} than for Ce^{4+} and, hence, dominate this part of the spectrum even in cases when Ce^{3+} content is small. Indeed, while dipole-forbidden peaks remain largely unchanged and Ce^{3+}-like for all the samples studied, there are clear spectral differences in the higher energy part of the $N_{4,5}$ multiplet as well as in the $M_{4,5}$-edge spectra (Fig. 3). Further studies are currently needed to verify this suggestion.

Our data also suggests that AGs with thicker ligaments have higher O deficiency. Indeed, the formation of the O vacancy in the CeO_2 lattice is accompanied by localization of two $4f$ electrons and an associated change in the oxidation state of two Ce atoms adjacent to the vacancy.[32] It is interesting to note that TEY XANES, which should effectively probe the entire thickness of (nonmetallic) ligaments ($\lesssim$10 nm),[31] reveals a large fraction of Ce atoms in the 3+ oxidation state in AG3 (Figs. 3 and 4). This is the oxidation state of Ce in Ce_2O_3. In contrast, selected-area electron diffraction [the inset in Fig. 1(d)] shows that ligaments in AG3 are comprised of crystallites with the crystallographic structure of full-density CeO_2, where Ce atoms should have a formal oxidation state of 4+.

The large fraction of Ce^{3+} revealed by XANES could be related to the presence of an amorphous phase of ceria in between CeO_2-like crystallites. In particular, Patsalas *et al.*[3] have reported experimental evidence that, in nanocrystalline films, the grain boundaries between CeO_2 crystallites contain O-deficient amorphous cerium oxides. Such an amorphous material between crystallites would not be readily revealed by diffraction-based techniques. However, our high-resolution TEM [Fig. 1(d)] did not reveal any significant amount of an amorphous material in AG3 to justify the high fraction of Ce^{3+} measured by XANES. An accurate quantitative estimate of the fraction of an amorphous material in AG3 based on TEM data is, however, not straightforward due to a spatial overlap of crystallites in thicker ligaments. These results could also be affected by electron-beam-induced recrystallization of disordered material during TEM imaging. Nevertheless, even if there were a significant fraction of a Ce^{3+}-like amorphous ceria phase, it would not explain why XANES spectra from AG3 indicate an almost pure Ce^{3+} character of the AG, while diffraction clearly shows the presence of CeO_2-like crystallites.

Our observations are, however, consistent with other reports,[4,34] showing that the relative concentration of Ce^{3+} rapidly increases with decreasing size of ceria nanoparticles below ~15 nm. For example, Wu *et al.*[4] have found that, in ceria particles with diameters of $\lesssim$3 nm, all Ce atoms are in the 3+ oxidation state, while nanoparticles remain with the fluorite structure, which is the same as the one of full-density CeO_2 but with two oxygen vacancies per unit cell (i.e., with 25% of oxygen removed from the structure). Hence, for small particles, the fraction of Ce atoms in the Ce^{3+} state could significantly exceed the surface-to-volume atomic ratio (which is ~40%–60% for a 3 nm ceria particle).

Similar results were also observed in our recent study of tin oxide AGs,[33] where Sn $3d$ XANES spectra from as-prepared AGs were characteristic of Sn^{2+} (as in romarchite SnO), while high-resolution TEM, selected-area electron diffraction, and x-ray diffraction revealed the crystallites with the rutile (cassiterite) phase of full-density SnO_2. These observations demonstrate that diffraction-based structural characterization of the crystallographic phase is not necessarily representative of the oxidation state of the metal atoms in the nanostructures, partly due to a large surface-to-volume atomic ratio in this class of materials. Similarly, the crystallographic phase of nanocrystals cannot be inferred from XANES data, and a combination of complementary characterization techniques is required for a complete description of material properties.

IV. SUMMARY

In summary, we have studied the atomic (by TEM) and electronic (by XANES spectroscopy) structures of ceria AGs

synthesized based on the epoxide-initiation gelation method. We have used atomic multiplet calculations to interpret the rich structure of Ce $M_{4,5}$- and $N_{4,5}$-edge XANES spectra. Results have shown that AGs with thicker ligaments, but with the same average size of CeO_{2-x} crystallites, have larger Ce^{3+} content. This finding has been attributed to a larger concentration of O vacancies in crystallites in AGs with thicker ligaments. Finally, our study shows that the electronic structure of sol-gel-derived nanoporous ceria strongly depends on preparation conditions, and more work is currently needed to gain a better control of the properties of ceria AGs in order for their technological potential to be fully exploited.

ACKNOWLEDGMENTS

The authors thank A. Gash, T. Baumann, J. Denlinger, F. M. F. de Groot, and J. Satcher, Jr. for useful discussions. This work was performed under the auspices of the U.S. DOE by the University of California, LLNL under Contract No. W-7405-Eng-48.

*Corresponding author. kucheyev@llnl.gov
†Present address: TDA Research, Inc., 4663 Table Mountain Dr., Golden, CO 80403. bclapsaddle@tda.com

[1] S. Cotton, *Lanthanide and Actinide Chemistry* (Wiley, West Sussex, 2006).
[2] See, for example, N. V. Skorodumova, R. Ahuja, S. I. Simak, I. A. Abrikosov, B. Johansson, and B. I. Lundqvist, Phys. Rev. B **64**, 115108 (2001), and references therein.
[3] P. Patsalas, S. Logothetidis, L. Sygellou, and S. Kennou, Phys. Rev. B **68**, 035104 (2003).
[4] L. Wu, H. J. Wiesmann, A. R. Moodenbaugh, R. F. Klie, Y. Zhu, D. O. Welch, and M. Suenaga, Phys. Rev. B **69**, 125415 (2004).
[5] F. Zhang, P. Wang, J. Koberstein, S. Khalid, and S.-W. Chan, Surf. Sci. **563**, 74 (2004).
[6] J. M. Herrmann, C. Hoang-Van, L. Dibansa, and R. Harivololona, J. Catal. **159**, 361 (1996).
[7] Y. Liu, H. L. Sun, Q. S. Liu, and H. F. Jin, J. Catal. **22**, 453 (2001).
[8] M. A. Thundathil, W. Lai, L. Noailles, B. S. Dunn, and S. M. Haile, J. Am. Ceram. Soc. **87**, 1442 (2003).
[9] C. Laberty-Robert, J. W. Long, E. M. Lucas, K. A. Pettigrew, R. M. Stroud, M. S. Doescher, and D. R. Rolison, Chem. Mater. **18**, 50 (2006).
[10] See, for example, reviews by N. Hüsing and U. Schubert, Angew. Chem., Int. Ed. **37**, 22 (1998); A. C. Pierre and G. M. Pajonk, Chem. Rev. (Washington, D.C.) **102**, 4243 (2002).
[11] B. J. Clapsaddle, D. W. Sprehn, A. E. Gash, and J. H. Satcher, Jr. (unpublished).
[12] F. de Groot, Coord. Chem. Rev. **249**, 31 (2005).
[13] T. M. Tillotson, W. E. Sunderland, I. M. Thomas, and L. W. Hrubesh, J. Sol-Gel Sci. Technol. **1**, 241 (1994).
[14] See, for example, J. Stöhr, *NEXAFS Spectroscopy* (Springer, Berlin, 1996).
[15] R. D. Cowan, *The Theory of Atomic Structure and Spectra* (University of California Press, Berkeley, 1981).
[16] B. T. Thole, G. van der Laan, J. C. Fuggle, G. A. Sawatzky, R. C. Karnatak, and J.-M. Esteva, Phys. Rev. B **32**, 5107 (1985).
[17] J. L. Dehmer, A. F. Starace, U. Fano, J. Sugar, and J. W. Cooper, Phys. Rev. Lett. **26**, 1521 (1971).
[18] J. Sugar, Phys. Rev. B **5**, 1785 (1972).
[19] T. Jo and A. Kotani, Phys. Rev. B **38**, 830 (1988).
[20] A. Kotani, H. Ogasawara, K. Okada, B. T. Thole, and G. A. Sawatzky, Phys. Rev. B **40**, 65 (1989).
[21] G. Strasser and F. P. Netzer, J. Vac. Sci. Technol. A **2**, 826 (1984).
[22] J. A. D. Matthew, G. Strasser, and F. P. Netzer, J. Phys. C **15**, L1019 (1982).
[23] O.-P. Sairanen, S. Aksela, and A. Kivimaki, J. Electron Spectrosc. Relat. Phenom. **72**, 327 (1995).
[24] Note that our theoretical $N_{4,5}$-edge spectrum for Ce^{4+} [Fig. 4(c)] is in agreement with some previous experimental studies of CeF_4 and CeO_2 (Refs. 21, 25, and 26).
[25] R. Haensel, P. Rabe, and B. Sonntag, Solid State Commun. **8**, 1845 (1970).
[26] G. Kalkowski, C. Laubschat, W. D. Brewer, E. V. Sampathkumaran, M. Domke, and G. Kaindl, Phys. Rev. B **32**, 2717 (1985).
[27] Photon flux values were estimated based on Au mesh current measurements and the photoelectron quantum efficiency values from Ref. 28.
[28] H. Henneken, F. Scholze, and G. Ulm, J. Appl. Phys. **87**, 257 (2000).
[29] B. L. Henke, E. M. Gullikson, and J. C. Davis, At. Data Nucl. Data Tables **54**, 181, 1993.
[30] Although accurate estimations of the TEY probing depth are challenging since it depends not only on energy but also on the material properties, previous studies have shown that the probing depth decreases with decreasing energy (Ref. 31).
[31] See, for example, B. H. Frazer, B. Gilbert, B. R. Sonderegger, and G. De Stasio, Surf. Sci. **537**, 161 (2003); M. Kasrai, W. N. Lennard, R. W. Brunner, G. M. Bancroft, J. A. Bardwell, and K. H. Tan, Appl. Surf. Sci. **99**, 303 (1996), and references therein.
[32] N. V. Skorodumova, S. I. Simak, B. I. Lundqvist, I. A. Abrikosov, and B. Johansson, Phys. Rev. Lett. **89**, 166601 (2002).
[33] S. O. Kucheyev, T. F. Baumann, P. A. Sterne, Y. M. Wang, T. van Buuren, A. V. Hamza, L. J. Terminello, and T. M. Willey, Phys. Rev. B **72**, 035404 (2005); T. F. Baumann, S. O. Kucheyev, A. E. Gash, and J. H. Satcher, Jr., Adv. Mater. (Weinheim, Ger.) **17**, 1546 (2005).
[34] S. Tsunekawa, K. Ishikawa, Z.-Q. Li, Y. Kawazoe, and A. Kasuya, Phys. Rev. Lett. **85**, 3440 (2000).